Extreme Poynting flux in the dayside thermosphere: Examples and statistics

D. Knipp,[1,2] S. Eriksson,[3] L. Kilcommons,[2] G. Crowley,[4] J. Lei,[1] M. Hairston,[5] and K. Drake[6]

Received 31 May 2011; revised 11 July 2011; accepted 12 July 2011; published 19 August 2011.

[1] With the launch of the Defense Meteorological Satellite Program F-15 spacecraft in late 1999, data for calculating Earth-directed, magnetospheric Poynting flux became available for the 09–21 solar local time sectors. We have assembled a data base for this key element of the upper atmosphere energy budget, for the interval 2000–2005. Here we briefly introduce the data set and show a subset that reveals a pattern of extreme Poynting flux deposition associated with a large east-west interplanetary magnetic field component. At such times the dayside high-latitude Poynting flux may exceed 170 mW/m^2—an order of magnitude above typical values. The likely source of these events is merging at the magnetopause flank and lobe. A significant fraction of these events occur with high speed solar wind. This pattern of extreme Poynting flux deposition has, to date, eluded detection. Energy deposition at these high rates is a likely source of previously reported, but poorly understood, near-cusp neutral density enhancements. **Citation:** Knipp, D., S. Eriksson, L. Kilcommons, G. Crowley, J. Lei, M. Hairston, and K. Drake (2011), Extreme Poynting flux in the dayside thermosphere: Examples and statistics, *Geophys. Res. Lett.*, *38*, L16102, doi:10.1029/2011GL048302.

1. Introduction

[2] Earth's upper atmosphere is powered by solar UV/EUV photons, energy deposition from the magnetosphere above, and tidal forcing from below. The highly time- and space-variable, magnetospheric component is supplied as precipitating particles and the flow of electromagnetic energy via Earth-directed, Poynting flux, $S_{||}$, where the subscript indicates the magnetic field-aligned component. We exploit low Earth orbit (LEO) measurements to investigate the source of order-of-magnitude enhancements in dayside $S_{||}$ deposition during large excursions of the east-west interplanetary magnetic field (IMF) component (B_y). For geospace applications, the Poynting vector, $\mathbf{S} = \mathbf{E} \times \delta\mathbf{B}/\mu_0$, is the result of the convection electric field, $\mathbf{E}$, crossed with $\delta\mathbf{B}$, the perturbation of the geomagnetic field with respect to the main field $\mathbf{B}_0$ [*Kelley et al.*, 1991]. The Poynting vector is a fundamental measure of electromagnetic energy transfer to a system. Poynting divergence, $\nabla \bullet \mathbf{S}$, manifests as Joule heating and kinetic energy of the ions that subsequently collide with atmospheric neutrals. This energy launches traveling atmospheric disturbances, drives ion and neutral upwelling, and supports neutral atmospheric expansion, all of which contribute to upper atmospheric disturbances.

[3] Global measures of $S_{||}$ for the Magnetosphere-Ionosphere-Thermosphere (M-I-T) system do not exist, however estimates of $S_{||}$ along the path of a LEO orbiting satellite(s) can aid in constraining the energy budget of such an electromagnetically driven system. Many researchers have used space-based $\mathbf{E}$ and $\mathbf{B}$ sensors for determining $S_{||}$ deposition, assuming quasi-static conditions (see summary by *Richmond* [2010]).

[4] *Gary et al.* [1995] reported average auroral zone $S_{||}$ values of 10–15 mW/m^2 for the Dynamics Explorer-2 satellite. During the B_z-negative phase of the April 2000 superstorm, *Huang and Burke* [2004] showed a single example of $S_{||}$ from Defense Meteorological Satellite Program (DMSP) F-13 exceeding 100 mW/m^2. *Korth et al.* [2005] found localized $S_{||}$ of ~50 mW/m^2 during a sustained, strongly northward IMF phase of the July 2000 superstorm. *Weimer*'s [2005] statistical patterns produce local dayside Joule heating rates of ~15 mW/m^2, for large IMF B_y values. In one instance, *Strangeway et al.* [2000] reported $S_{||}$ as high as 120 mW/m^2 at 4000 km with strong IMF B_y (~40 nT), and verified that the $S_{||}$ is dominant over the particle energy input to the cusp-region ionosphere. These studies were unable to draw enough samples from the dayside region to reveal the patterns shown here from DMSP measurements.

2. Data Sources

[5] Data from space environment sensors aboard DMSP spacecraft quantify magnetospheric energy input to the upper atmosphere. Relevant to this study are data from the magnetometer, ion drift meter (IDM), and the retarding potential analyzer (RPA). The F-15 triaxial fluxgate magnetometer is mounted on a 5-m boom, reducing its susceptibility to spacecraft-generated contamination. We use magnetic perturbation vector values provided by the Air Force Research Laboratory, calculated in the spacecraft frame. Differences between measured and International Geomagnetic Reference Field (IGRF) values of magnetic fields at the spacecraft locations, $\delta\mathbf{B} = \mathbf{B}_{\text{meas}} - \mathbf{B}_{\text{IGRF}}$, are calculated [*Huang and Burke*, 2004]. A further adjustment is made each half orbit by fitting a high-order polynomial to the residuals outside of

[1]Aerospace Engineering Sciences, University of Colorado at Boulder, Boulder, Colorado, USA.
[2]High Altitude Observatory, National Center for Atmospheric Research, Boulder, Colorado, USA.
[3]Laboratory for Atmospheric and Space Physics, University of Colorado at Boulder, Boulder, Colorado, USA.
[4]Atmospheric and Space Technology Research Associates, LLC, Boulder, Colorado, USA.
[5]Center for Space Sciences, University of Texas at Dallas, Richardson, Texas, USA.
[6]Valdez International Corporation, Colorado Springs, Colorado, USA.

0094-8276/11/2011GL048302

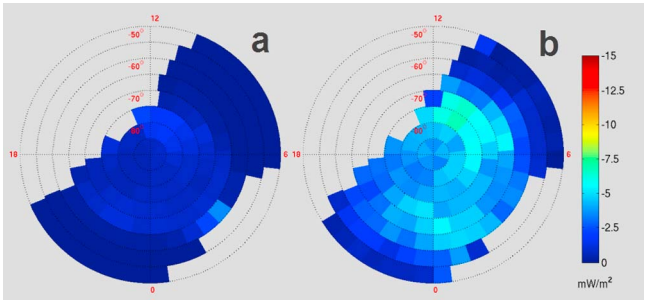

Figure 1. Southern Hemisphere binned and equal -area -averaged $S_{||}$ for 2000–2005 covering −50° Mlat to −90° Mlat. (a) Averaged, quietest day of month; (b) averaged, most disturbed day of month. Negative values on the color bar indicate Earth-directed $S_{||}$.

the auroral oval and subtracting the fit to remove the remaining baseline. The IDM measures horizontal cross-track and vertical components of plasma drifts, and the RPA measures ion temperatures and the in-track component of plasma drift [*Rich and Hairston*, 1994]. Preprocessing of the IDM and RPA data removes Earth's co-rotation velocity. The electric field vector values are determined using $\mathbf{E} = -\mathbf{V} \times \mathbf{B}_{IGRF}$. We calculate $S_{||}$, using the following steps, where x refers to the along-track component and y refers to the cross-track component:

$$\mathbf{S} = (\mathbf{E} \times \delta\mathbf{B})/\mu_0$$

$$\mathbf{S}_{||} = \left(E_x \delta B_y - E_y \delta B_x\right)/\mu_0$$

System geometry dictates the energy flow is primarily Earth-directed (negative). Our calculations show that $S_{||}$ is field aligned to within 10% above 55° Mlat.

3. Results

[6] Figure 1 shows polar views of DMSP $S_{||}$ averaged into approximately equal area bins in the southern hemisphere (SH). There, the sun-synchronous orbit covers the largest swaths of magnetic local time (MLT) as the magnetic pole moves beneath the satellite. The data represent the most geomagnetically quiet (Figure 1a) and disturbed (Figure 1b) day of each month during 2000–2005 according to the Kp index. Each image contains ~1000 passes. Some bins at the edge of coverage represent less than 5 passes. Average values of $S_{||}$ are ~0.5 mW/m^2 for quiet times and ~3.0 mW/m^2 for disturbed times. Applying these values to the region above 50° Mlat gives hemispheric Poynting deposition of ~30 GW and 180 GW respectively for quiet and disturbed times, in good agreement with the range of Joule heating rates discussed by *Knipp et al.* [2004], *Weimer* [2005] and *McHarg et al.* [2005]. Figure 1 provides the backdrop for studying enhanced $S_{||}$ during large IMF B_y.

[7] Snapshots, in Figure 2, of the $S_{||}$ at the DMSP-15 track are in MLT-magnetic latitude (Mlat) format for the northern hemisphere (NH) during an event with large swings in the east-west IMF on August 24, 2005 (see Figure 2a). The orbit track color-coding, and the magnitude of the excursion from the track, indicate the intensity of the down-going $S_{||}$. In Figure 2b the satellite crosses a post-noon deposition region where $S_{||} \sim 20$ mW/m^2 while the solar wind speed was modest (460 km/s) and the IMF had a westward component ($B_Y \sim +8$ nT). Subsequently a significant solar wind shock arrived at Earth, conveying solar wind speeds of 550 km/s or more. The post-shock $S_{||}$, located slightly equatorward of the previous measurement, exceeded 120 mW/m^2 (Figure 2c). At that time B_y was ~+21 nT. Figure 2d illustrates the $S_{||}$ during the passage of an interplanetary coronal mass ejection (ICME) with speed of ~640 km/s, when the B_y component was ~−20 nT and $S_{||}$ reached ~170 mW/m^2. During the event, the most intense $S_{||}$ moved from post-noon (B_y positive) to pre-noon (B_y negative) in the NH, consistent with the migration of NH high-latitude merging site(s) under the influence of IMF B_z+ and a varying east-west IMF component [*Luhmann et al.*, 1984; *Reiff and Burch*, 1985]. During southern hemisphere (SH) crossings, which occur on the nightside, $S_{||}$ was negligible throughout the interval.

[8] The DMSP data shows that large IMF B_y excursions, typically accompanied by high speed solar wind, are associated with enhanced dayside $S_{||}$. Figures 3a–3d show plots of the maximum $S_{||}$ for each DMSP F-15 2000–2005 polar pass meeting the condition: IMF $|B_y| > 10$ nT. Figures 3a and 3b display the cases for IMF B_z+, while the Figures 3c and 3d show the IMF B_z-cases. The $S_{||}$ values exceeding 75 mW/m^2 and 100 mW/m^2 are shown with cross-like symbols and triangles, respectively. Based on the Svalgaard-Mansurov effect [*Svalgaard*, 1968; *Mansurov*, 1969] and *Luhmann et al.*'s [1984] geometry, the IMF B_y-associated $S_{||}$ should maximize on the dusk side of noon in the north and the dawn side in the south for $B_y > 0$, and vice-versa for $B_y < 0$. We combine the data accordingly and find that large values of $S_{||}$ for NH B_y− and SH B_y+ (Figures 3a and 3c) tend to cluster near 10 MLT, while large values for $S_{||}$ NH B_y+ and SH B_y− (Figures 3b and 3d) tend to be closer to noon. We expect that given a global distribution for $S_{||}$ (which we cannot achieve with DMSP measurements), the $S_{||}$ values for the latter case would be centered in the post noon region.

[9] A few large values of $S_{||}$ appear in the nightside for IMF B_z-cases. These are likely associated with substorms and, perhaps, subauroral polarization streams. The 101-

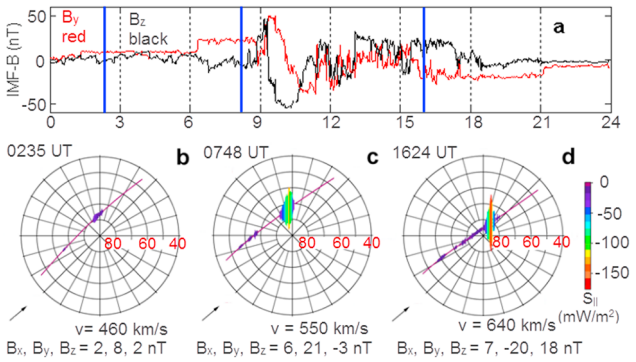

Figure 2. (a) Interplanetary magnetic field data; and NH $S_{||}$ along three DMSP F15 passes for 24 August 2005. The polar plots are in magnetic coordinates. The arrow at lower left indicates the direction of spacecraft motion. (b) $S_{||}$ after a weak shock with IMF $B_y \sim 8$ nT. (c) Post-shock $S_{||}$ while the IMF B_y was ~21 nT and $B_z \sim -3$ nT. (d) ICME $S_{||}$ while the IMF B_y was ~−20 nT and $B_z \sim 18$ nT.

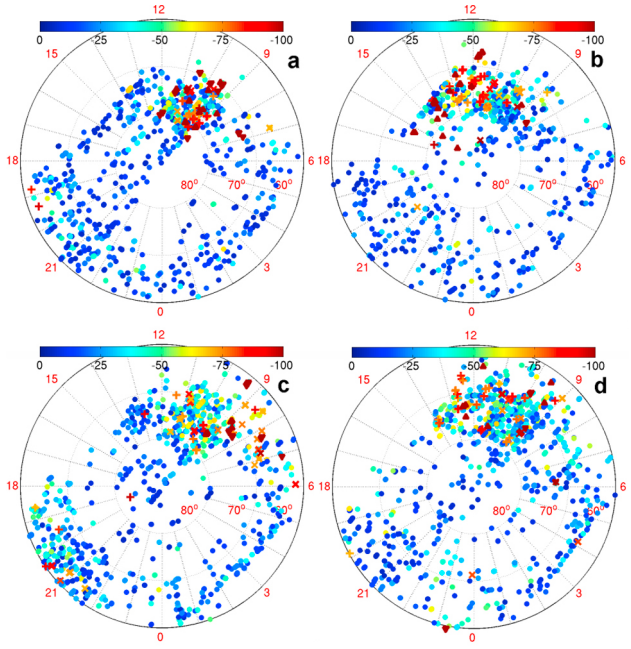

Figure 3. Survey of Maximum $S_{||}$ during IMF $B_y > 10$ nT events from 2000–2005. (top) The maximum $S_{||}$ for intervals of $B_z > 0$ nT and $|B_y| > 10$ nT. (a) NH IMF B_y- and SH IMF B_y+ events. (b) NH IMF B_y+ and SH IMF B_y- events. (bottom) The maximum $S_{||}$ for intervals of $B_z < 0$ nT and $|B_y| > 10$ nT. (c) NH IMF B_y- and SH IMF B_y+ events. (d) NH IMF B_y+ and SH IMF B_y- events. $S_{||}$ in excess of 75mW/m^2 is highlighted by colored "+" (NH) and "x" (SH). $S_{||}$ exceeding 100 mW/m^2 is highlighted by colored upward triangles (NH) and colored downward triangles (SH).

minute DMSP F-15 orbit sub-samples these events in both time and space. Thus, large-to-extreme dayside $S_{||}$ is probably more common than Figure 3 indicates. Note that DMSP F-15 does not pass through the post noon to dusk sector, so our counts are skewed in favor of pre-noon events.

4. Discussion and Conclusions

[10] The comparison of background $S_{||}$ deposition for quiet and disturbed intervals from DMSP F-15 in Figure 1 shows, as expected, the disturbed intervals having a generally increased level of $S_{||}$. In addition the disturbed-time plot suggests a coherent, enhanced dayside energy deposition region compared to patchy structure on the nightside. This enhancement maps to regions of flank and lobe-mantle magnetopause merging. *Li et al.* [2011] modeled these deposition regions for large IMF clock angle ($|B_y| > B_z$), and argue the deposition becomes more elongated in longitude as the clock angle increases and becomes more intense as the solar wind speed or the IMF magnitude increases.

[11] Individual satellite passes (Figure 2) from a period of increasing solar wind speed and rotating IMF B_y suggest that both speed and extreme B_y excursions play a role in the preferential dayside deposition. Figure 3 shows that intervals of large IMF B_y are often associated with localized extreme $S_{||}$ deposition. In the ~1500 passes represented in Figure 3, there are numerous instances of an order-of-magnitude increase in dayside $S_{||}$ (>75 mW/m^2) when the east-west IMF is large, regardless of the sign of IMF B_Z. We note that when IMF is southward, the extent of the dayside events is more equatorward, consistent with the tendency for an expanded polar cap convection system.

[12] Although the longitudinal extent of the $S_{||}$ in Figures 2 and 3 cannot be determined from the DMSP measurements, *Maynard* [2005] reported that newly opened field lines resulting from cusp merging may couple to the ionosphere at MLT locations extending as much as three hours away from local noon. Modeling by *Vennerstrom et al.* [2005] revealed that, as the east-west IMF magnitude grows, field aligned currents (FACs) migrate in an IMF-dependent manner. Observations by *Anderson et al.* [2008] showed a similar result and inferred the associated $\mathbf{E} \times \mathbf{B}$ flow channels. *Eriksson et al.* [2008] determined that, as the IMF B_y rotated from large positive to large negative values during an ICME passage, strong FACs and $\mathbf{E} \times \mathbf{B}$ flow channels moved from the evening side, across noon, to the morning side. Juxtaposition of intense electric fields associated with high-speed ion flow channels and strong B_y driven FACs produces the extreme $S_{||}$ in the dayside high latitudes. A sunlit ionosphere is crucial to providing FAC closure via an ionospheric Pedersen current [*Li et al.*, 2011].

[13] The triangles in Figure 3 indicate the many instances of dayside $S_{||}$ approaching or even exceeding the value associated with superstorm level (100 mW/m^2) [*Huang and Burke*, 2004]. The number of events is noteworthy given that only ten superstorms (Dst < −250) occurred during the interval 2000–2005. Several factors support this preferential dayside deposition: (1) solar-enhanced conductance is located on the dayside; (2) the dayside magnetic merging configurations develop quickly and need not process energy through the magnetotail in a substorm/storm process; (3) the magnetopause-merging process is active during northward and southward IMF.

[14] The large dayside $S_{||}$ events are important for M-I-T coupling. *Crowley et al.* [2010] showed a longitudinally-extended arc of dayside Joule heating along with uplifted neutral density in the same NH region for the event in Figure 2b. The data revealed thermospheric uplift at the location of the strong energy source. Likewise, strong uplift was modeled in the SH cusp region, but not on the nightside, consistent with the absence of any nightside high-latitude energy source near the satellite track in the winter hemisphere. The B_y-dominated energy deposition is likely related to statistical cusp and dayside high-latitude neutral density enhancements reported by *Lühr et al.* [2004] and *Moe and Moe* [2008]. The influence of east-west IMF excursions has additional ramifications. *Immel et al.* [2006] found that B_y exerts significant control over the development and subsequent equatorward transport of composition disturbances during periods of heightened geomagnetic activity.

[15] Large IMF components tend to be present at the leading edge of co-rotating interaction regions and during ICMEs. In the case of ICMEs, and the most geoeffective subset of these, magnetic clouds, the deposition can be of long duration. The duration may be longer if the transient structure has a lengthy leading sheath region with large in-the-ecliptic IMF components and neutral or northward B_z. In fact, we were motivated to undertake this study because satellite orbit determination algorithms revealed

events with poorly specified, enhanced neutral density having many of these IMF characteristics (B. Bowman, personal communication, 2008).

[16] Consistent with *Strangeway et al.* [2005] our preliminary check on energy flux from precipitating particles shows particle energy deposition to be much less than that from $S_{||}$. However, there may be a substantial associated flux of low energy electrons (~0.5 keV) that could effectively energize matter in the upper F-region. Our investigations of the association of large $S_{||}$ events with low energy electrons and the sensitivity of the extreme dayside $S_{||}$ event to solar wind speed, seasonal effects, and other IMF orientations are ongoing.

[17] In this paper we focus on large dayside Poynting flux deposition that has eluded detection. Prior to this study, limitations in sensing $S_{||}$ have heretofore allowed a significant mode of M-I-T coupling to go undetected in its fullest sense. Here, we show Poynting deposition during intervals of large east-west IMF when substantial energy, exceeding 100 mW/m^2, can be deposited in the dayside high-latitude M-I-T system. Intervals that might otherwise be considered geomagnetically quiet in terms of geomagnetic storm indices are, in fact, rather active for the high-latitude dayside thermosphere. The likely effects on the dayside thermosphere are significant, yet have largely been unexplored.

[18] **Acknowledgments.** We are grateful to G. Wilson who provided the DMSP magnetometer data and F. Rich who removed the magnetic field background. R. Heelis, A. Richmond and B. Emery provided many useful discussions. DK, GC, JL, and KD were supported by AFOSR MURI award FA9550-07-1-0565. MH was supported by grants from: NASA NNX07AT186 and NSF ATM-637791. SE was supported by NASA grant NNX10AQ45G GC was also supported by NSF GEM Award ATM-0703335. DK was also supported by a National Research Council fellowship. IMF data are from ACE and CDAWeb. Quiet and disturbed days are provided by World Data Center for Geomagnetism (C1), Copenhagen. NCAR is supported by the National Science Foundation.

[19] The Editor thanks Daniel Weimer and an anonymous reviewer for their assistance in evaluating this paper.

References

Anderson, B. J., et al. (2008), Statistical Birkeland current distributions from magnetic field observations by the Iridium constellation, *Ann. Geophys.*, *26*, 671, doi:10.5194/angeo-26-671-2008.

Crowley, G., D. J. Knipp, K. A. Drake, J. Lei, E. Sutton, and H. Lühr (2010), Thermospheric density enhancements in the dayside cusp region during strong B_Y conditions, *Geophys. Res. Lett.*, *37*, L07110, doi:10.1029/2009GL042143.

Eriksson, S., M. R. Hairston, F. J. Rich, H. Korth, Y. Zhang, and B. J. Anderson (2008), High-latitude ionosphere convection and Birkeland current response for the 15 May 2005 magnetic storm recovery phase, *J. Geophys. Res.*, *113*, A00A08, doi:10.1029/2008JA013139.

Gary, J. B., R. A. Heelis, and J. P. Thayer (1995), Summary of field-aligned Poynting flux observations from DE2, *Geophys. Res. Lett.*, *22*, 1861, doi:10.1029/95GL00570.

Huang, C. Y., and W. J. Burke (2004), Transient sheets of field-aligned current observed by DMSP during the main phase of a magnetic superstorm, *J. Geophys. Res.*, *109*, A06303, doi:10.1029/2003JA010067.

Immel, T. J., G. Crowley, C. L. Hackert, J. D. Craven, and R. G. Roble (2006), Effect of IMF By on thermospheric composition at high and middle latitudes: 2. Data comparisons, *J. Geophys. Res.*, *111*, A10312, doi:10.1029/2005JA011372.

Kelley, M. C., D. J. Knudsen, and J. F. Vickrey (1991), Poynting flux measurements on a satellite: A diagnostic tool for space research, *J. Geophys. Res.*, *96*, 201, doi:10.1029/90JA01837.

Knipp, D. J., et al. (2004), Solar direct and indirect thermospheric heating sources for solar cycles 21–23, *Sol. Phys.*, *224*, 495, doi:10.1007/s11207-005-6393-4.

Korth, H., et al. (2005), High-latitude electromagnetic and particle energy flux during an event with sustained strongly northward IMF, *Ann. Geophys.*, *23*, 1295–1310, doi:10.5194/angeo-23-1295-2005.

Li, W., D. Knipp, J. Lei, and J. Raeder (2011), The relation between dayside local Poynting flux enhancement and cusp reconnection, *J. Geophys. Res.*, doi:10.1029/2011JA016566, in press.

Luhmann, J. G., R. J. Walker, C. T. Russell, N. U. Crooker, J. R. Spreiter, and S. S. Stahara (1984), Patterns of potential magnetic field merging sites on the dayside magnetopause, *J. Geophys. Res.*, *89*, 1739, doi:10.1029/JA089iA03p01739.

Lühr, H., M. Rother, W. Köhler, P. Ritter, and L. Grunwaldt (2004), Thermospheric up-welling in the cusp region: Evidence from CHAMP observations, *Geophys. Res. Lett.*, *31*, L06805, doi:10.1029/2003GL019314.

Mansurov, S. M. (1969), New evidence of a relationship between magnetic fields in space and on Earth, *Geomagn. Aeron., Engl. Transl.*, *9*, 622.

Maynard, M. C. (2005), Coupling the solar-wind/IMF to the ionosphere through the high latitude cusps, *Surv. Geophys.*, *26*(1–3), 255, doi:10.1007/s10712-005-1882-4.

McHarg, M., F. Chun, D. Knipp, G. Lu, B. Emery, and A. Ridley (2005), High-latitude Joule heating response to IMF inputs, *J. Geophys. Res.*, *110*, A08309, doi:10.1029/2004JA010949.

Moe, K., and M. M. Moe (2008), The high-latitude thermospheric mass density anomaly: A historical review and a semi-empirical model, *J. Atmos. Sol. Terr. Phys.*, *70*, 794, doi:10.1016/j.jastp.2007.10.007.

Reiff, P. H., and J. L. Burch (1985), IMF By-dependent plasma flow and Birkeland currents in the dayside magnetosphere: 2. A global model for northward and southward IMF, *J. Geophys. Res.*, *90*, 1595, doi:10.1029/JA090iA02p01595.

Rich, F. J., and M. Hairston (1994), Large-scale convection patterns observed by DMSP, *J. Geophys. Res.*, *99*, 3827, doi:10.1029/93JA03296.

Richmond, A. D. (2010), On the ionospheric application of Poynting's theorem, *J. Geophys. Res.*, *115*, A10311, doi:10.1029/2010JA015768.

Strangeway, R. J., C. T. Russell, C. W. Carlson, J. P. McFadden, R. E. Ergun, M. Temerin, D. M. Klumpar, W. K. Peterson, and T. E. Moore (2000), Cusp field-aligned currents and ion outflows, *J. Geophys. Res.*, *105*(A9), 21,129, doi:10.1029/2000JA900032.

Strangeway, R. J., R. E. Ergun, Y.-J. Su, C. W. Carlson, and R. C. Elphic (2005), Factors controlling ionospheric outflows as observed at intermediate altitudes, *J. Geophys. Res.*, *110*, A03221, doi:10.1029/2004JA010829.

Svalgaard, L. (1968), Sector structure of the interplanetary magnetic field and daily variations of the geomagnetic field at high latitudes, *Geophys. Pap. R-6*, Dan. Meteorol. Inst., Copenhagen.

Vennerstrom, S., T. Moretto, L. Rastätter, and J. Raeder (2005), Field-aligned currents during northward interplanetary magnetic field: Morphology and causes, *J. Geophys. Res.*, *110*, A06205, doi:10.1029/2004JA010802.

Weimer, D. R. (2005), Improved ionospheric electrodynamic models and application to calculating Joule heating rates, *J. Geophys. Res.*, *110*, A05306, doi:10.1029/2004JA010884.

G. Crowley, Atmospheric and Space Technology Research Associates, LLC, 5777 Central Ave., Ste. 221, Boulder, CO 80301, USA.

K. Drake, Valdez International Corporation, 1490 Garden of the Gods Rd., # B, Colorado Springs, CO 80907, USA.

S. Eriksson, Laboratory for Atmospheric and Space Physics, University of Colorado at Boulder, 1234 Innovation Dr., Boulder, CO 80303, USA.

M. Hairston, Center for Space Sciences, University of Texas at Dallas, 800 West Campbell Rd., WT15, Richardson, TX 75080, USA.

L. Kilcommons and D. Knipp, High Altitude Observatory, National Center for Atmospheric Research, 3080 Center Green Dr., Boulder, CO 80302, USA. (knipp@ucar.edu)

J. Lei, Aerospace Engineering Sciences, University of Colorado at Boulder, 429 UCB, Boulder, CO 80309, USA.